Supplementary Information

Title: Heterogeneous impacts of fire-sourced ozone (O_3) pollution on global crop yields in the future climate scenarios

Authors: Rui Li[a, b], Dongmei Tang[a, b, *], Yumeng Shao[a], Yining Gao[a], Hongfang Zhao[a *]

Affiliations: [a] *Key Laboratory of Geographic Information Science of the Ministry of Education, School of Geographic Sciences, East China Normal University, Shanghai, 200241, PR China*

[b] *Institute of Eco-Chongming (IEC), 20 Cuiniao Road, Chenjia Town, Chongming District, Shanghai, 202162, China*

*** Corresponding author**

Prof. Tang (dmtang@geo.ecnu.edu.cn) and Prof. Zhao (hfzhao@geo.ecnu.edu.cn)

Number of pages: 14

Number of figures: 10

Number of tables: 1

Three statistical indicators including determination coefficient (R^2), root mean square error (RMSE), and mean absolute error (MAE) were applied to validate the modelling performances of ambient MDA8 O_3 concentration (Li et al., 2019; Li et al., 2023). P_i and O_i represent the predicted and observed concentrations, respectively. SSR and SST represent the regression sum of squares and total sum of squares, respectively. The detailed equations are as follows:

$$R^2 = \frac{SSR}{SST} \quad (1)$$

$$RMSE = \sqrt{\frac{\sum_{i=1}^{N}(P_i - O_i)^2}{N}} \quad (2)$$

$$MAE = \sum_{i=1}^{N}\left|P_i - O_i\right| \quad (3)$$

Besides, some redundant variables were also removed in the final model because it might degrade the predictive accuracy of the multi-stage model.

Table S1 The updated AOT40 response function for major four crops.

	Equation	References
Maize	RY=-0.0058AOT40+1	[1]
Rice	RY=-0.009489AOT40+1	[2]
Spring wheat	RY=-0.0205AOT40+1	[3]
Winter wheat	RY=-0.0205AOT40+1	[3]

Figure S1 The workflow of wildfire-induced O_3 concentration and crop yield loss estimates.

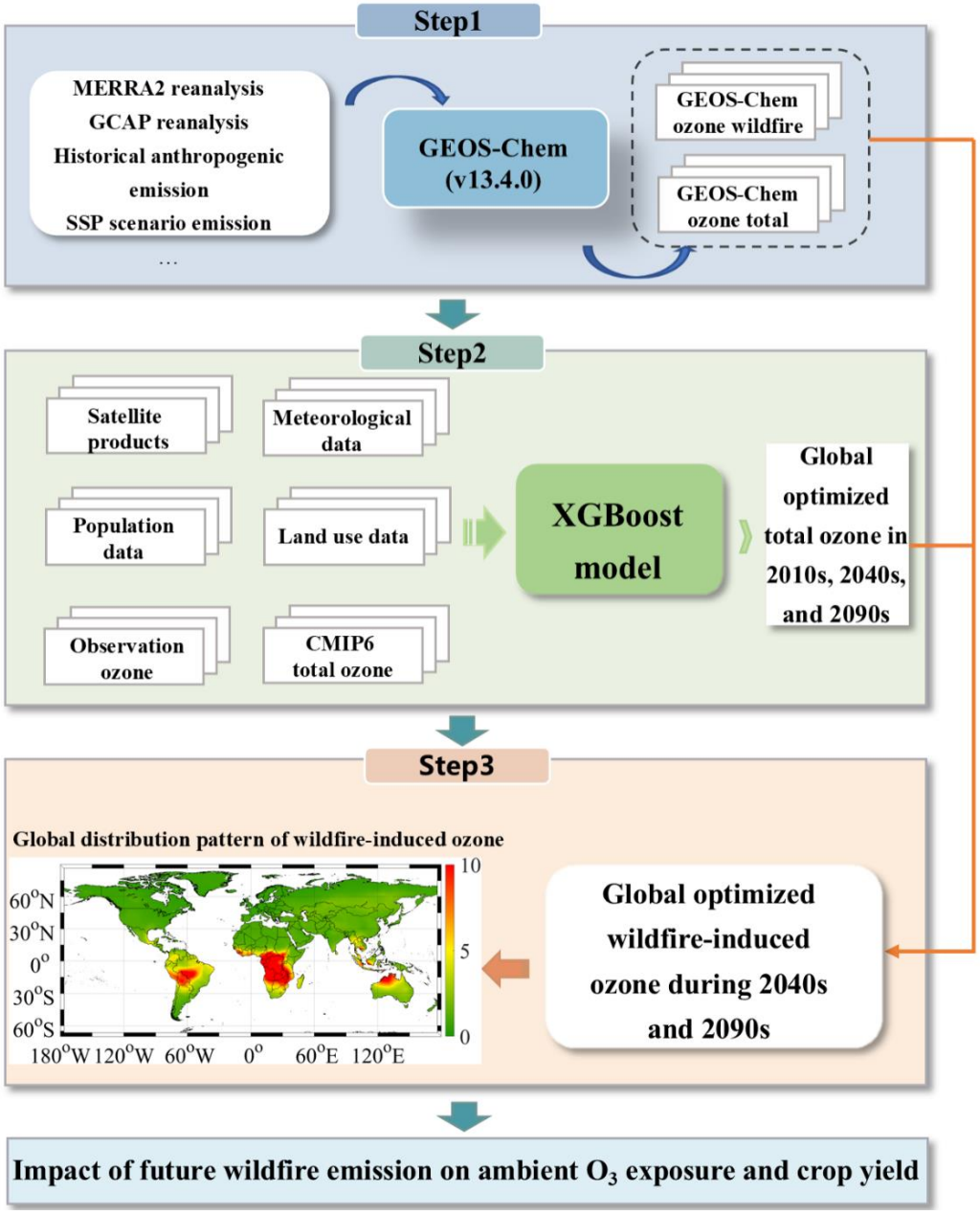

Figure S2 The predictive accuracy of MDA8 O_3 concentration at the global scale (a). The relationship between fire-sourced MDA8 O_3 level and K^+ concentration (b).

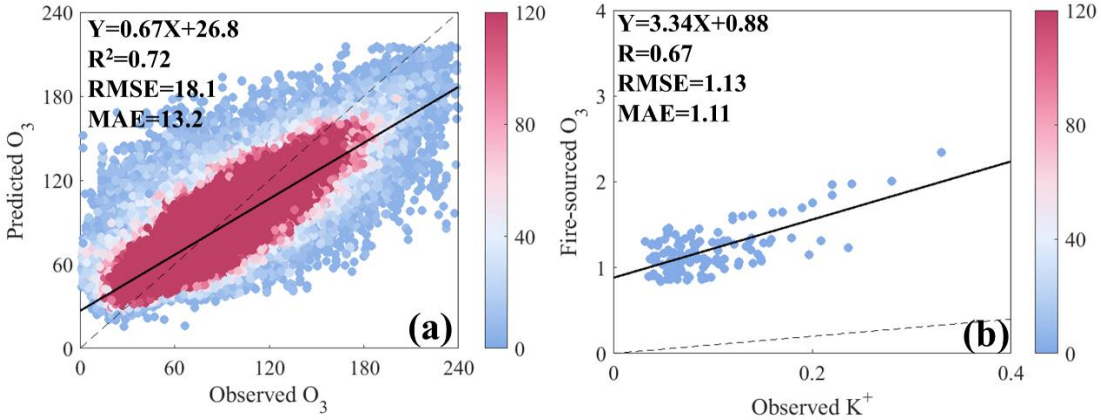

Figure S3 The global variations of wildfire-induced 8-h O_3 levels (Unit: μg/m^3) in SSP1-2.6 (a), SSP3-7.0 (b), and SSP5-8.5 (c) scenarios during 2090s. The spatial distributions of wildfire-related 8-h O_3 concentrations (Unit: μg/m^3) in different regions during 2090s (d). US, SA, and SS represent the United States, South America, and Sub-Sahara Africa, respectively.

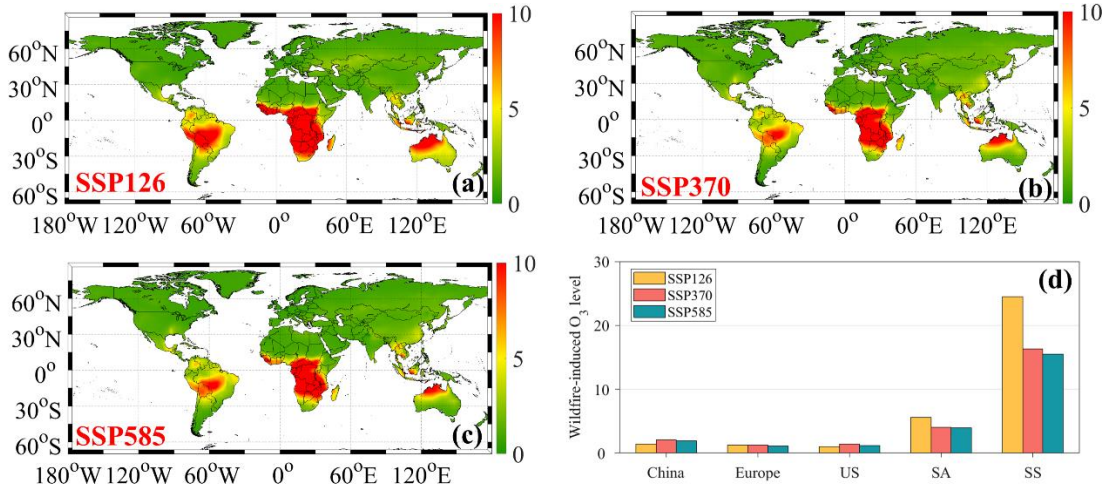

Figure S4 The global variations of wildfire-induced O_3-related rice yield losses (Unit: t/km^2) during historical (a), SSP1-2.6 (b), SSP3-7.0 (d), and SSP5-8.5 (e) scenarios during 2040s, respectively. The spatial variations of wildfire-induced rice yield losses (Unit: t/km^2) in major regions during 2040s. US, SA, and SS represent the United States, South America, and Sub-Sahara Africa, respectively.

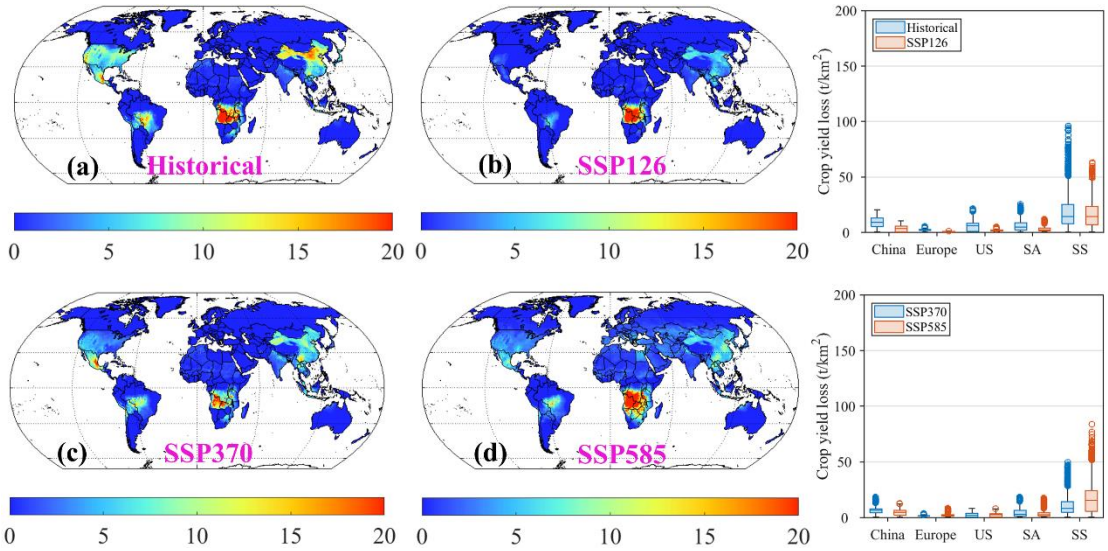

Figure S5 The global variations of wildfire-induced O_3-related spring wheat yield losses (Unit: t/km^2) during historical (a), SSP1-2.6 (b), SSP3-7.0 (d), and SSP5-8.5 (e) scenarios during 2040s, respectively. The spatial variations of wildfire-induced spring wheat yield losses (Unit: t/km^2) in major regions during 2040s. US, SA, and SS represent the United States, South America, and Sub-Sahara Africa, respectively.

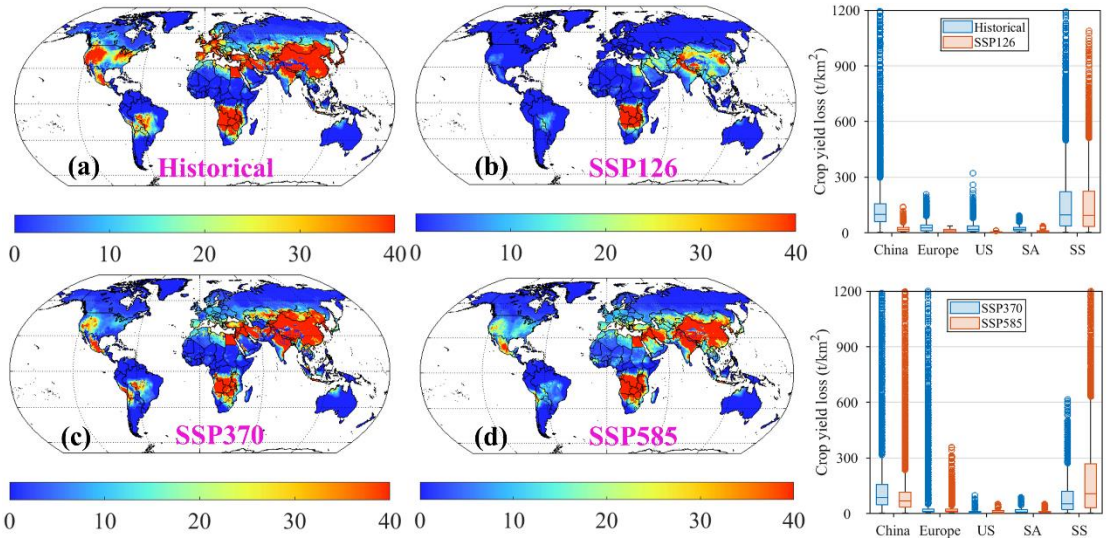

Figure S6 The global variations of wildfire-induced O_3-related winter wheat yield losses (Unit: t/km^2) during historical (a), SSP1-2.6 (b), SSP3-7.0 (d), and SSP5-8.5 (e) scenarios during 2040s, respectively. The spatial variations of wildfire-induced winter wheat yield losses (Unit: t/km^2) in major regions during 2040s. US, SA, and SS represent the United States, South America, and Sub-Sahara Africa, respectively.

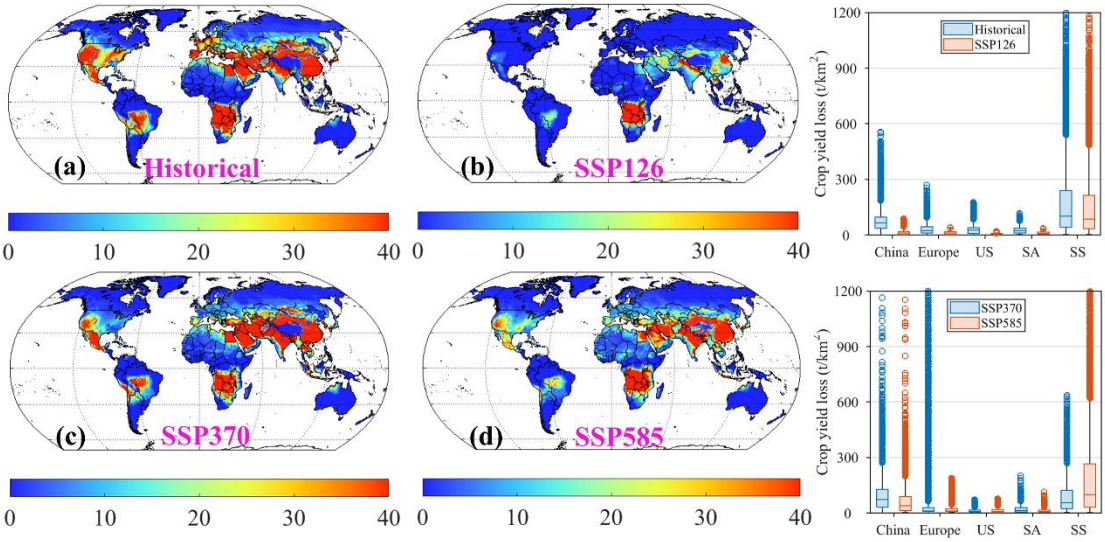

Figure S7 The global variations of wildfire-induced O_3-related maize yield losses (Unit: t/km^2) during SSP1-2.6 (a), SSP3-7.0 (b), and SSP5-8.5 (c) scenarios during 2090s, respectively. The global difference of wildfire-induced maize yield losses (Unit: t/km^2) in different SSP scenarios during 2090s. US, SA, and SS represent the United States, South America, and Sub-Sahara Africa, respectively.

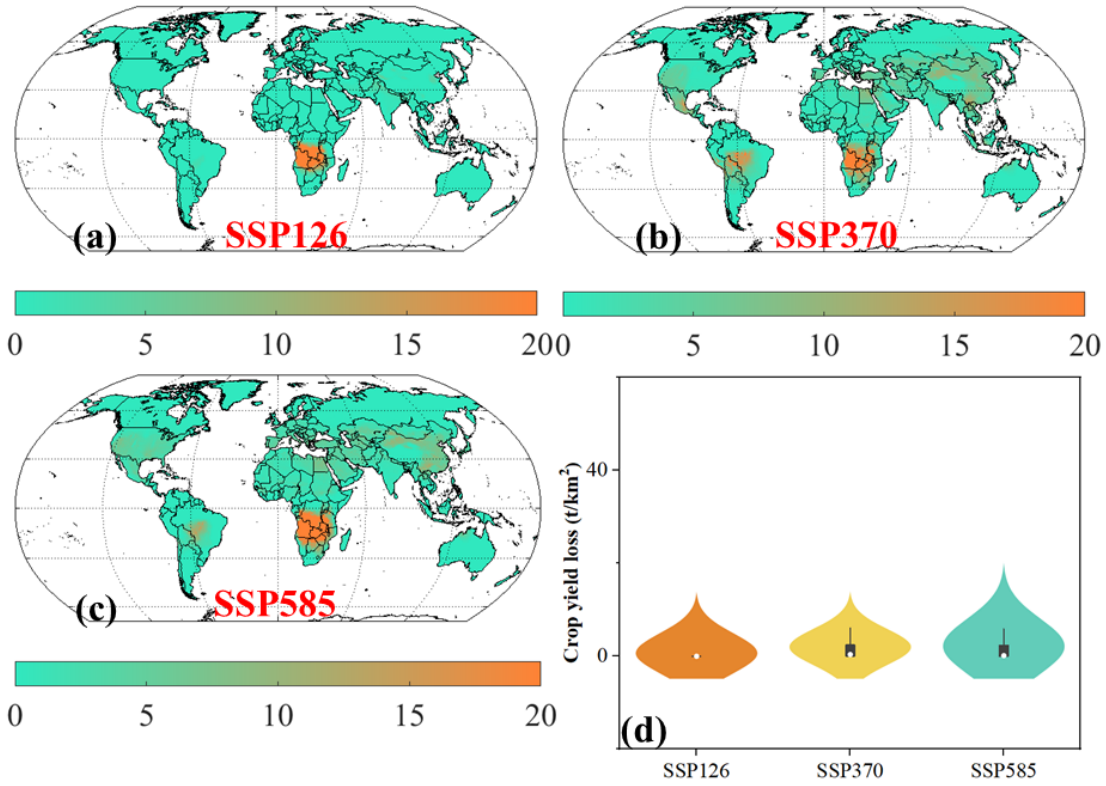

Figure S8 The global variations of wildfire-induced O_3-related rice yield losses (Unit: t/km^2) during SSP1-2.6 (a), SSP3-7.0 (b), and SSP5-8.5 (c) scenarios during 2090s, respectively. The global difference of wildfire-induced rice yield losses (Unit: t/km^2) in different SSP scenarios during 2090s. US, SA, and SS represent the United States, South America, and Sub-Sahara Africa, respectively.

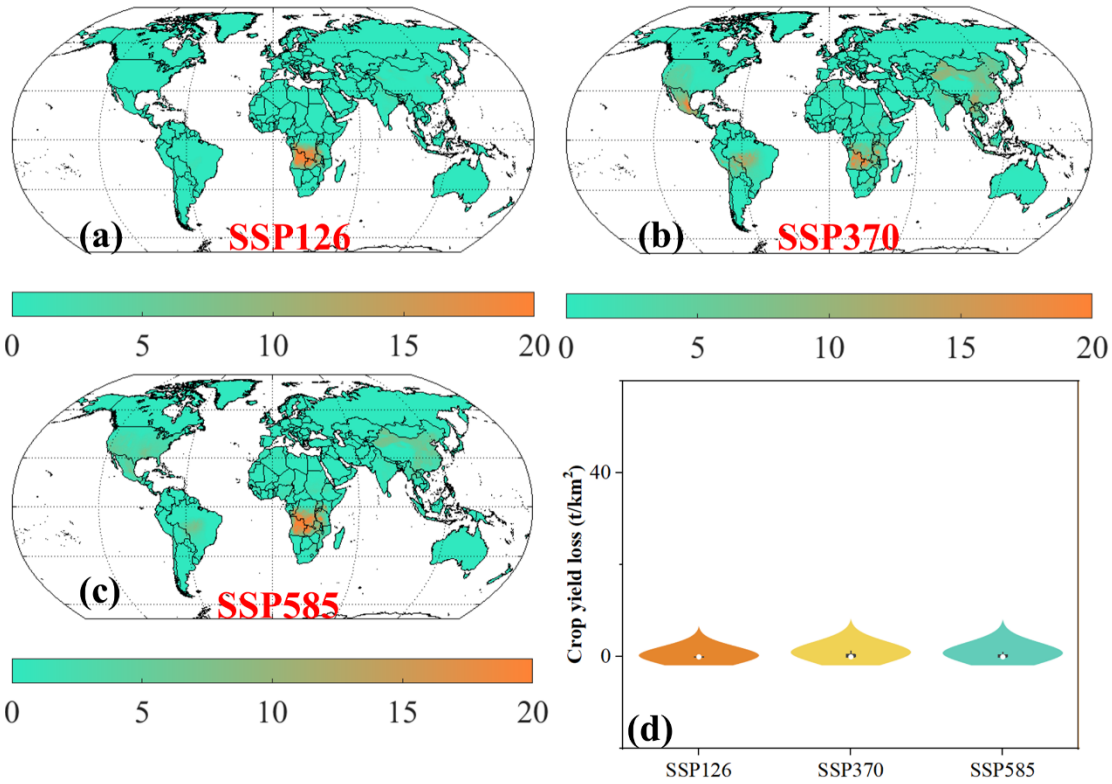

Figure S9 The global variations of wildfire-induced O_3-related spring wheat yield losses (Unit: t/km^2) during SSP1-2.6 (a), SSP3-7.0 (b), and SSP5-8.5 (c) scenarios during 2090s, respectively. The global difference of wildfire-induced spring wheat yield losses (Unit: t/km^2) in different SSP scenarios during 2090s. US, SA, and SS represent the United States, South America, and Sub-Sahara Africa, respectively.

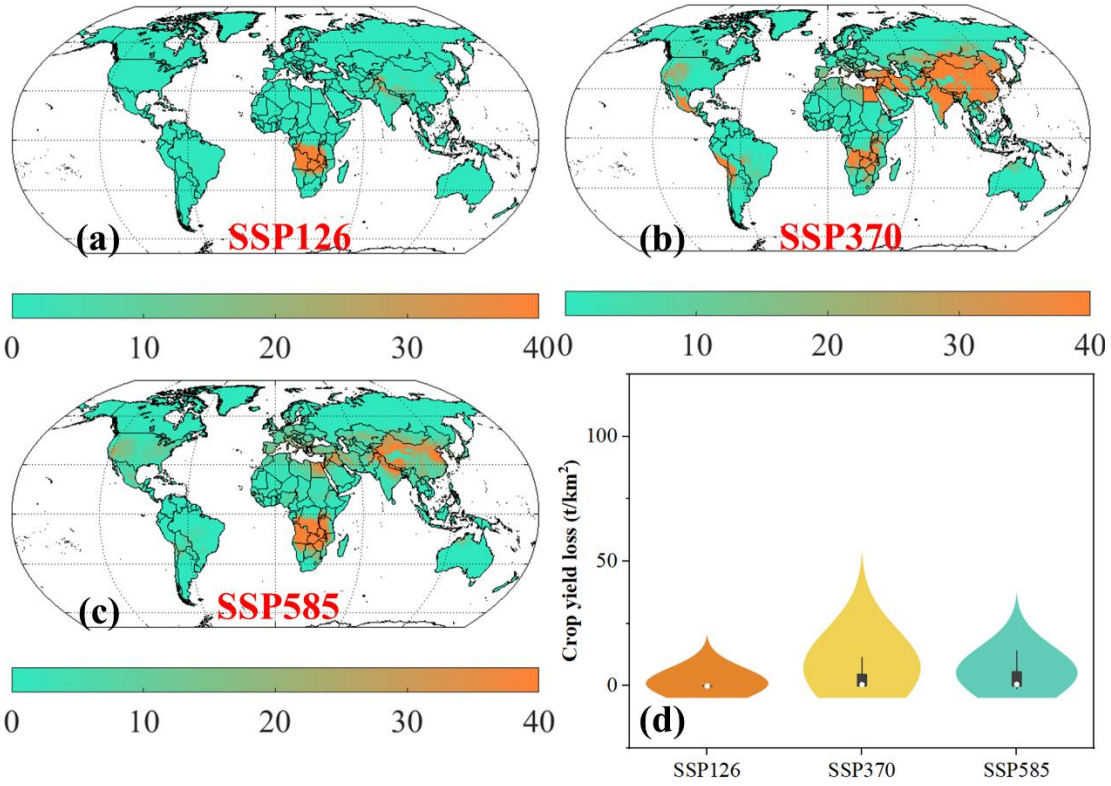

Figure S10 The global variations of wildfire-induced O_3-related winter wheat yield losses (Unit: t/km^2) during SSP1-2.6 (a), SSP3-7.0 (b), and SSP5-8.5 (c) scenarios during 2090s, respectively. The global difference of wildfire-induced winter wheat yield losses (Unit: t/km^2) in different SSP scenarios during 2090s. US, SA, and SS represent the United States, South America, and Sub-Sahara Africa, respectively.

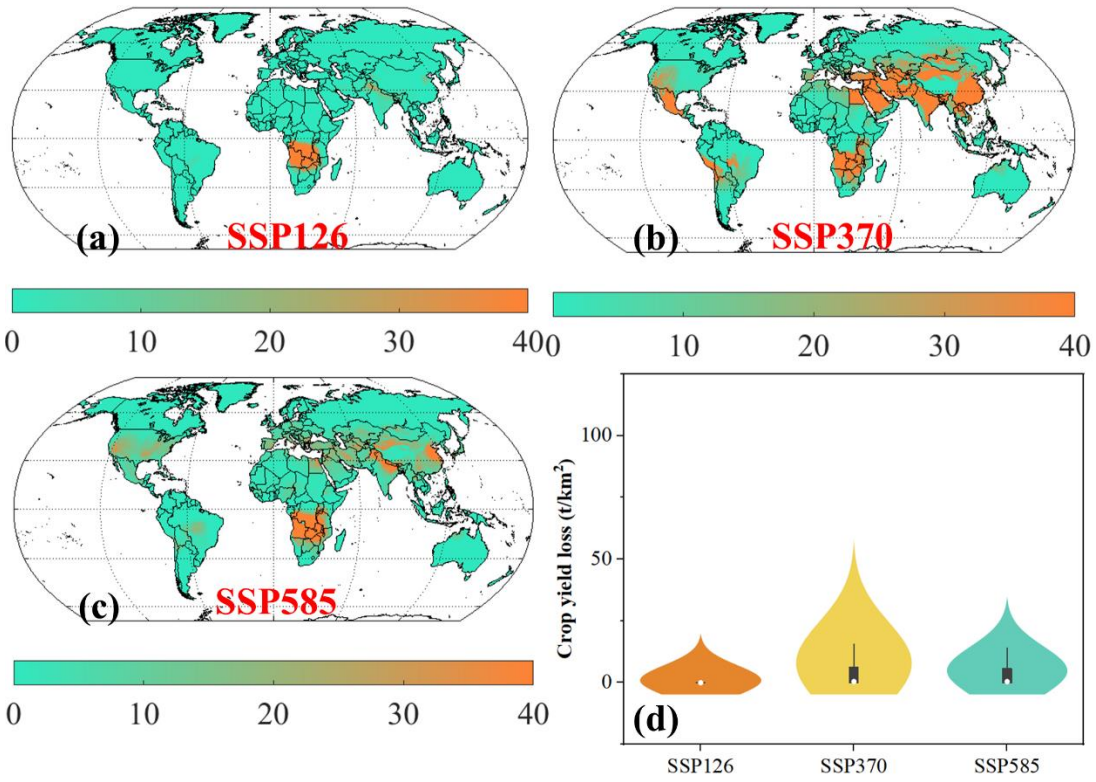

References

1. Peng, J.; Shang, B.; Xu, Y.; Feng, Z.; Pleijel, H.; Calatayud, V., Ozone exposure-and flux-yield response relationships for maize. *Environmental pollution* **2019,** *252*, 1-7.

2. Wang, X.; Mauzerall, D. L., Characterizing distributions of surface ozone and its impact on grain production in China, Japan and South Korea: 1990 and 2020. *Atmospheric Environment* **2004,** *38*, (26), 4383-4402.

3. Feng, Z.; Kobayashi, K.; Li, P.; Xu, Y.; Tang, H.; Guo, A.; Paoletti, E.; Calatayud, V., Impacts of current ozone pollution on wheat yield in China as estimated with observed ozone, meteorology and day of flowering. *Atmospheric Environment* **2019,** *217*, 116945.